



Numerical simulations for fluid dynamics and temperature patterns in membrane distillation channels

M. Shakaib¹ · M. Ehtesham-ul Haque¹

Received: 7 August 2018 / Accepted: 12 June 2019 / Published online: 20 June 2019
© Springer-Verlag GmbH Germany, part of Springer Nature 2019

Abstract

The effect of spacer orientation on flow behavior is studied at different spacer filament spacings using Computational Fluid Dynamics (CFD) technique. At high inlet velocity / Reynolds number the flow becomes transient and vorticity magnitude increases in a major portion of the two channels. The temperature and heat flux in this case also vary in time. The comparison of various spacer geometrical arrangements/orientations shows that the arrangements in which the spacer filaments are opposite to the membrane layers are more suitable due to higher heat transfer rates. Further appropriate turbulence models for predicting flow and heat transfer behavior in membrane channels are also proposed.

Nomenclature

C_p	Specific heat (J/kg·K)
d_f	Filament diameter (m)
d_h	Hydraulic diameter (m)
h	Heat transfer coefficient (W/m ² ·K)
h_{ch}	Channel height (m)
k_t	Thermal conductivity (W/m·K)
$k-\omega$	Turbulence model, turbulent kinetic energy (m ² /s ²) and specific dissipation rate (1/s)
L	Channel length (m)
l_f	Mesh length / filament spacing (m)
Nu	Nusselt number
Pr	Prandtl number
q_w	Heat flux (W/m ²)
Re	Reynolds number
u_{av}	Average velocity (m/s)
T_b	Bulk temperature (K)
T_m	Temperature at membrane surface (K)
u	x-component of velocity (m/s)
v	y-component of velocity (m/s)
x	x-coordinate (m)
y	y-coordinate (m)
ρ	Density (kg/m ³)
μ	Viscosity (kg/m·s)
ε	Voidage of feed or permeate channel

ε_m	Voidage of membrane
θ	Flow attack angle

1 Introduction

Membrane distillation (MD) is one of the desalination processes that have gained popularity in the past few years. The reasons are low mechanical power input, high recovery rates, and percentage salt rejections even at high feed salt concentrations. The separation in this process takes place due to the gradient of vapor pressure or temperature of the product and the saline feed streams. A small portion of liquid converts into vapor and permeates through pores of the hydrophobic membrane. The vapor changes its phase in the cold channel and is collected in liquid form as a product. Among the problems that restrict the use of membrane distillation systems on relatively large-scale are scaling, fouling and temperature polarization [1, 2]. Scaling refers to saturation and precipitation of chemical species whereas fouling is a build-up of particulates, biofilms and organic matter near the membrane surface. Temperature polarization is a reduction in temperature difference across the membrane surfaces when compared to the difference of the bulk temperatures. The decrease in temperature gradient across the membrane surface decreases the effective vapor pressure gradient thereby reducing product water. To mitigate the above problems, better membrane material or membrane preparation technique can be used or the design of membrane module can be modified. An important component of the spiral wound and flat sheet membrane modules is net-type spacer which creates flow channels, promotes mixing

✉ M. Shakaib
mshakaib@neduet.edu.pk; mshakaib@live.com

¹ Department of Mechanical Engineering, NED University of Engineering and Technology, Karachi, Pakistan

and enhances heat and mass transfer. Suitably designed and placed spacers in feed and permeate channels can also reduce the problems of fouling and concentration/temperature polarization.

A number of papers have appeared in the literature related to the membrane distillation process. The review papers [3, 4] discussed the heat and mass transfer concepts involved in the membrane distillation, recent developments related to new modules, membrane preparation, and influence of operating conditions. Another paper [5] reviewed research studies that utilized CFD method to study momentum, heat and mass transport in conventional and modified membrane distillation module. Fimbres-Weihs and Wiley [6] reviewed papers related to fluid flow and mass transfer modeling in spiral wound membranes. The authors suggested that optimal spacer designs can be obtained using the CFD technique. The effect of spacer geometry on temperature and concentration polarization has been reported in several studies. As examples, Katsandri [7] performed the CFD simulations at different hydrodynamic angles. An angle of 45° was found more suitable for minimizing temperature polarization. The research of Chang et al. [8] showed that the local heat and the mass flux values near the membrane surface continuously increase and decrease due to the repeating nature of the spacer. Seo et al. [9] proposed a symmetric circular-zigzag spacer with a larger diameter to be better for the MD process. Martínez et al. [10, 11] experimentally examined the influence of open separator, coarse screen separator and fine screen separator and indicated that the coarse screen separator results in more turbulence and decreases temperature polarization. Phattaranawik et al. [12, 13] tested numerous spacers and found that permeate flow increases about 30–40% when the spacer is used for direct contact membrane distillation. A spacer with a hydrodynamic angle of 90° was indicated to be the most suitable. Chernyshov et al. [14] compared spacers of two different shapes: round filaments and twisted filaments for an air-gap membrane distillation process. A hydrodynamic angle of 45° in case of round filament spacers and an angle of 30° for twisted filaments were identified to be suitable. The research work of Cipollina et al. [15, 16] also showed that the spacer considerably alters the flow and temperature distributions in the MD channel. The computational work of Sharif et al. [17] using OpenFOAM CFD code proposed that the use of a 3-layer spacer in the membrane distillation flow passages results in less frictional loss and uniform temperature distribution. Soukane et al. [18] discussed the effect of feed flow structure on the direct contact membrane distillation membrane process. The analysis indicated a major effect of flow recirculation and stagnant zones on module performance. Yu et al. [19] compared the baffled and non-baffled geometries for a hollow fiber module. The comparison showed that the baffled module shows significant improvement at higher temperatures. Various shapes for baffles were considered by Ahadi et al.

[20]. It was found that triangular shaped baffles provide more uniform temperature distribution near the membrane surface. The study of Guan et al. [21] explored the effect of brine salinity on the membrane distillation process. The analysis revealed that high feed temperature and Reynolds number range 500–2000 helps prevention of supersaturation which can reduce membrane scaling. The model developed by Eleiwi et al. [22] determined the performance of the MD process under steady or intermittent energy supply conditions. The model results were found to agree with experimental results. The previous work of present authors included simulations for steady fluid flow behavior in the MD process at different spacer orientations [23]. The flow in a spacer-filled channel becomes unstable and transient at a relatively lower value of Reynolds number when compared to a plane channel. The critical value of Reynolds number at which flow becomes transient/transitional depends on various factors such as the spacer filament spacing and filament height but it ranges from 150 to 800 as known from previous studies. In this flow regime, the unsteady simulation in a CFD solver shows variation of velocity, temperature, and heat flux within the channel with time even though the boundary conditions are constant. In this research, transient simulations are conducted and flow behavior and temperatures are obtained for different orientations and inter-filament spacings.

An approach used by researchers for simulating transitional flow fields in membrane channels is to use turbulence models and solve for the mean or time-averaged flow quantities. Among the models that have been utilized for membrane processes, are Standard $k-\varepsilon$ [24, 25], RNG $k-\varepsilon$ [26–28], and Realizable $k-\varepsilon$ [29, 30]. The present work also aims to suggest the turbulence models that can yield more accurate results for flow in membrane channels.

2 Modeling procedure

Membranes configurations predominantly used are spiral-wound, hollow-fiber, and plate-frame. In spiral-wound and plate-frame configurations, net-type spacers are often placed in the feed and permeate channels which greatly affect the temperature and concentration polarization and membrane fouling. This paper includes CFD simulations for various spacer arrangements and filament spacings at different velocities. A schematic for a section of membrane module containing membrane layer, feed and permeate channels and the various arrangements/orientations considered are shown in Fig. 1. Commonly used net-type spacer consists of two sets of filaments; one overlapping on the other. In 2D simulations, only the effect of one set of filaments which is in the transverse direction is examined. Four different spacer orientations that were found suitable in our earlier paper [23] are studied. The details are (i) Type 1: transverse filaments are placed in the

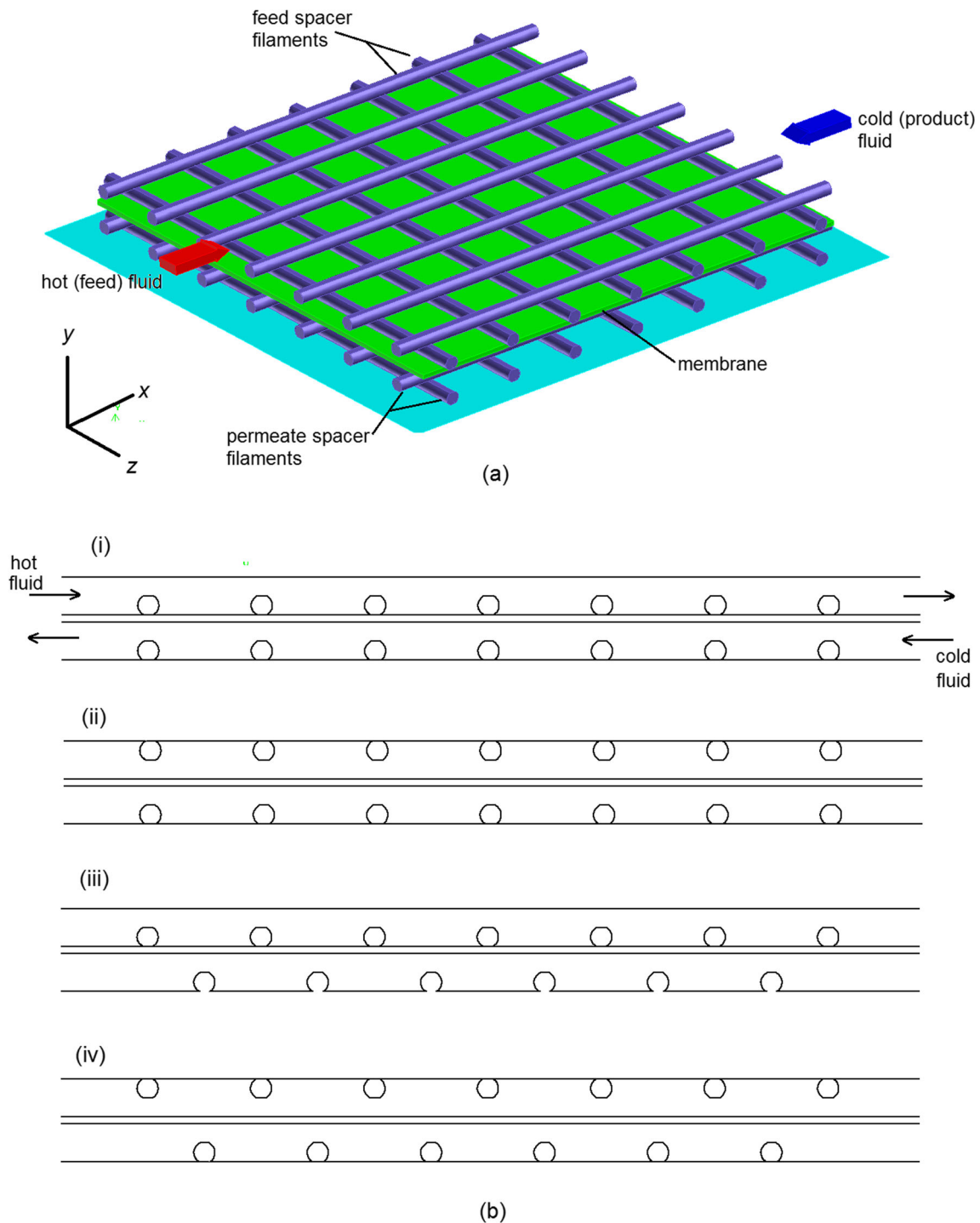


Fig. 1 a Schematic of membrane distillation module b various spacer orientations (i) Type 1 (ii) Type 2 (iii) Type 1-st (iv) Type 2-st.

bottom portion in both the channels and are inline (ii) Type 2: spacer filaments of both channels are on the opposite side of the membrane i.e. filaments of hot channel are in top portion whereas filaments of cold channel are in bottom portion and filaments are inline (iii) Type 1-st: transverse filaments are in the bottom portion in both the channels and are staggered (iv) Type 2-st: filaments are on the opposite side of the membrane and have staggered placement. The computational domains

consist of a hot (feed), a cold (product) channel and a membrane layer. The height of both, the feed and the permeate channels is 1 mm whereas membrane thickness is 0.2 mm which are the usual dimensions of different components of the membrane module. The effect of mesh length or spacing between filaments (l_f) is also determined on unsteady flow behavior. The value of l_f considered is 3 or 4.5 mm. The domain is split into a number of finite volumes of quad shape

as shown in Fig. 2. The number of cells is about 50,000 which provide grid-independent results. For example, heat flux difference is less than 1% when the number of cells is increased up to 120,000 for Type 1 configuration at maximum velocity (0.35 m/s). In many of the incompressible flow devices including membrane modules, volume flow rate or velocity is known at the inlet and pressure can be assumed at the outlet. The boundary conditions are, therefore ‘velocity inlet’ for the inlet and ‘pressure outlet’ for the outlet for both hot and cold fluids. The two fluids flow in the opposite direction that is the hot fluid flows from left to right and cold fluid flows left to right. The spacer filaments and top and bottom module surfaces are assumed as a wall. In the membrane distillation process, a fraction of high-temperature fluid vaporizes due to the vapor pressure gradient and passes through the membrane. The vaporization or permeate flow rate in the membrane distillation process is around $75 \text{ kg/m}^2\cdot\text{h}$ [31]. This corresponds to the vapor velocity of about $2 \times 10^{-5} \text{ m/s}$ which is much lower than the feed velocity. From previous studies [24, 26, 32] it is known that the velocity profiles in the cross-flow channel are not affected due to low permeation. Since heat transfer strongly depends on hydrodynamic conditions, it can be inferred that temperature patterns in the spacer-filled channels will be uninfluenced due to permeate flow. The flow and thermal behavior thus depend only on spacer dimensions and placement, flow and fluid properties (e.g. feed velocity, viscosity, and density). The membrane, hence, in the present work is considered as a non-permeable wall. Due to the assumption of membrane impermeability, the vapor/saturation

pressures are not determined or specified as no flow moves from one channel to another. The fluid is water whose density ρ , specific heat C_p , thermal conductivity k_f are constant while viscosity μ depends on temperature. The flow pattern is examined at various velocities that are in the range of 0.15–0.35 m/s which corresponds to Reynolds number range of 300–850. The considered velocities or Reynolds number represent the typical flow conditions in MD modules [10, 12]. Reynolds number is defined as:

$$\text{Re} = \frac{\rho u_{av} d_h}{\mu} \quad (1)$$

$$d_h = \frac{4 \times \text{Volume of flow channel}}{\text{Wetted surface area}} \quad (2)$$

In Eq. (1) u_{av} is average velocity and d_h is the hydraulic diameter.

For comparison with experimental results Prandtl number Pr and Nusselt Number Nu are also calculated:

$$\text{Pr} = \frac{\mu C_p}{k_f} \quad (3)$$

$$\text{Nu} = \frac{h d_h}{k} \quad (4)$$

The heat transfer coefficient h is calculated as:

$$h = \frac{q_w}{T_b - T_m} \quad (5)$$

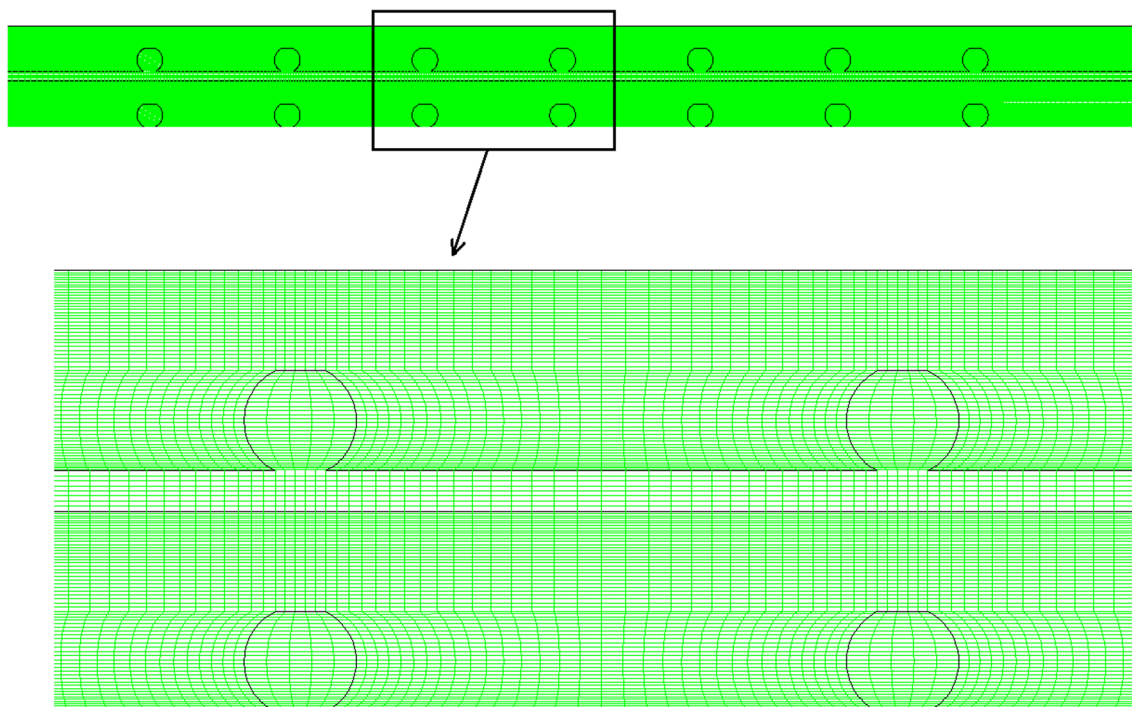


Fig. 2 Computational grid for simulations

In Eq. (5) q_w is heat flux, T_b is the bulk temperature and T_m is the local temperature at the membrane.

For fluid dynamics and heat transfer modeling, the governing equations are the conservation of mass, momentum, and energy which have a differential form for viscous and rotational flow [33]. These Eqs. (6)–(9) are given as:

$$\frac{\partial u}{\partial x} + \frac{\partial v}{\partial y} = 0 \tag{6}$$

$$\rho \left(\frac{\partial u}{\partial t} + u \frac{\partial u}{\partial x} + v \frac{\partial u}{\partial y} \right) = -\frac{\partial p}{\partial x} + 2 \frac{\partial}{\partial x} \left(\mu \frac{\partial u}{\partial x} \right) + \frac{\partial}{\partial y} \left[\mu \left(\frac{\partial u}{\partial y} + \frac{\partial v}{\partial x} \right) \right] \tag{7}$$

$$\rho \left(\frac{\partial v}{\partial t} + u \frac{\partial v}{\partial x} + v \frac{\partial v}{\partial y} \right) = -\frac{\partial p}{\partial y} + \frac{\partial}{\partial x} \left[\mu \left(\frac{\partial v}{\partial x} + \frac{\partial u}{\partial y} \right) \right] + 2 \frac{\partial}{\partial y} \left(\mu \frac{\partial v}{\partial y} \right) \tag{8}$$

$$\rho C_p \left(\frac{\partial T}{\partial t} + u \frac{\partial T}{\partial x} + v \frac{\partial T}{\partial y} \right) = k_t \left(\frac{\partial^2 T}{\partial x^2} + \frac{\partial^2 T}{\partial y^2} \right) \tag{9}$$

These equations are solved using code ANSYS FLUENT. Second-order upwind scheme is used to discretize the differential equations and SIMPLE procedure is used to couple velocity and pressure fields.

The present results are compared with correlations/equations given in previous experimental studies. Equation (10) was developed through experiments by Phattaranawik et al. [13] for the spacer-filled membrane distillation process while Eq. (12) was developed by Schock and Miquel [34] for mass transfer in reverse osmosis membrane channel. Due to heat and mass transfer analogy, it can be acceptable to apply correlations of reverse osmosis process for heat transfer in membrane distillation. For validation of numerical results in this study, the Nusselt numbers calculated using Eq. (4) are compared with Nusselt numbers obtained using the Eqs. (10) and (12).

$$Nu = \alpha \left[4.36 + \frac{0.036 Re Pr (d_h/L)}{1 + 0.0011 (Re Pr (d_h/L))^{0.8}} \right] \tag{10}$$

where

$$\alpha = 1.88 \left(\frac{d_f}{h_{ch}} \right)^{-0.039} (\sin\theta)^{1.33} \times \exp \left(-4.05 \left(\left[\ln \left(\frac{\varepsilon}{\varepsilon_m} \right) \right]^2 \right) \right) \tag{11}$$

$$Nu = 0.065 Re^{0.875} Pr^{0.25} \tag{12}$$

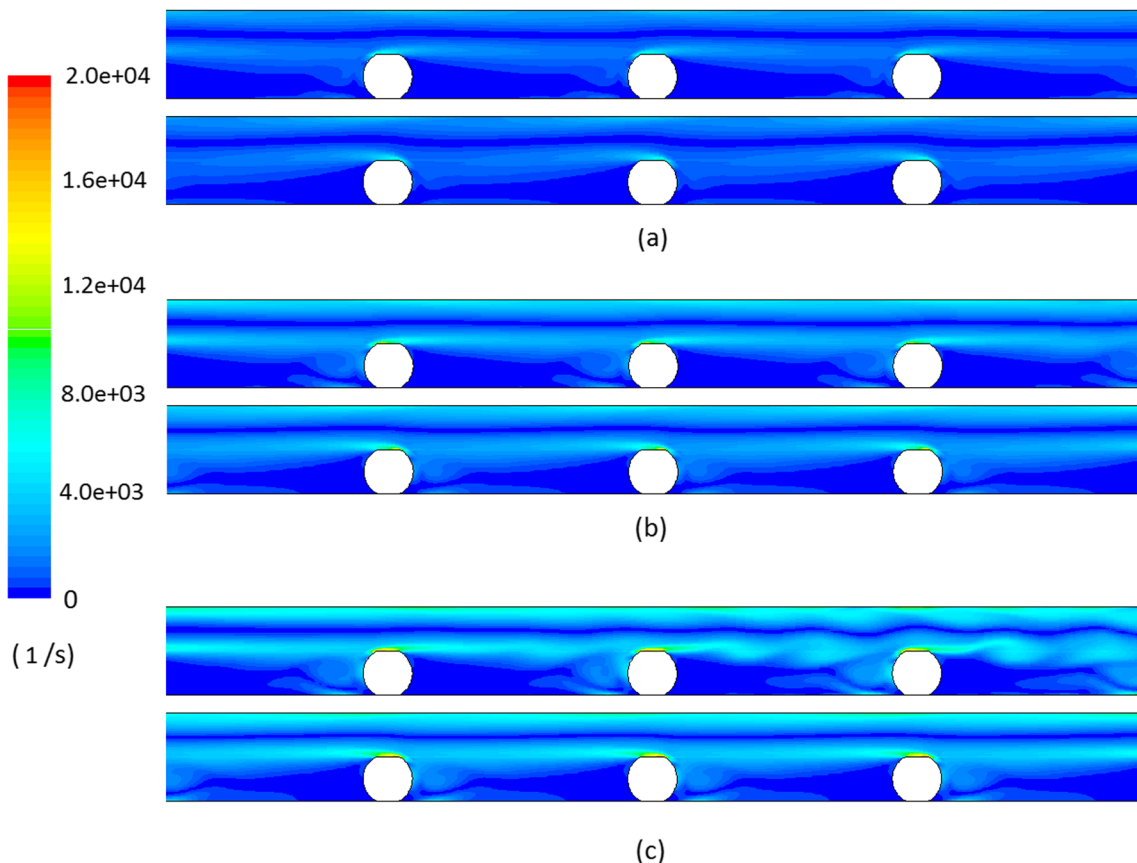


Fig. 3 Vorticity contours in inline type arrangement, $l_f=3$ mm, inlet velocity equal to a 0.15 m/s b 0.25 m/s c 0.35 m/s

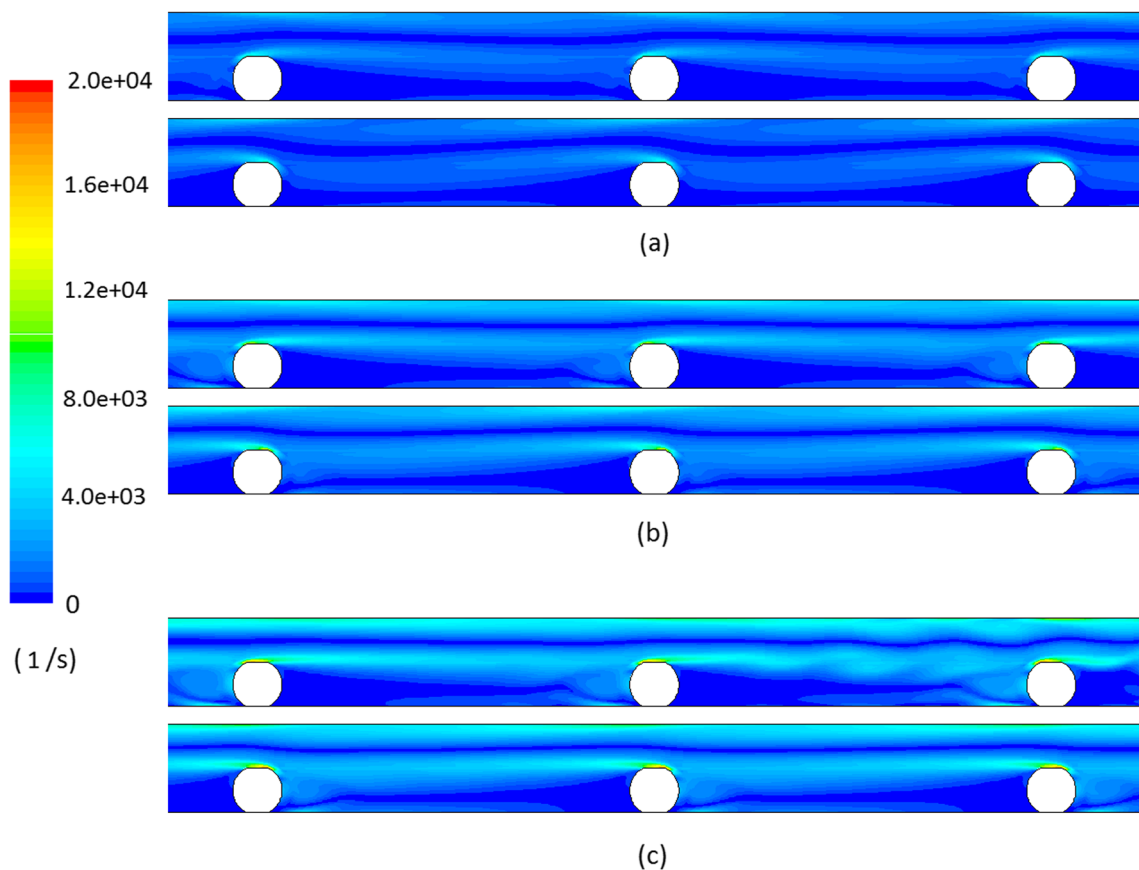


Fig. 4 Flow (vorticity) patterns in inline configuration, $l_f = 4.5$ mm, inlet velocity equal to **a** 0.15 m/s **b** 0.25 m/s **c** 0.35 m/s

3 Results and discussion

The flow patterns are discussed in terms of vorticity, a parameter which indicates the velocity gradient. As shown in Fig. 3,

the vorticity is higher in the top portion of the channel and near the filaments due to high-velocity variation. This behavior is noticed at all the considered velocities in this study. At high inlet velocity ($u_{av} = 0.35$ m/s), the flow becomes unsteady and

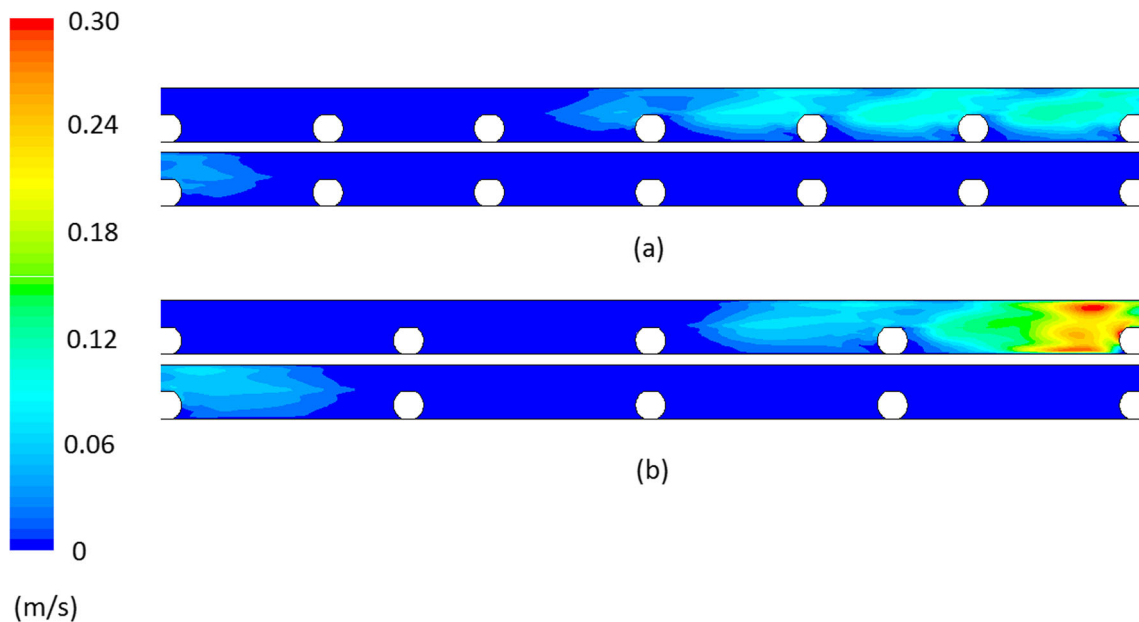
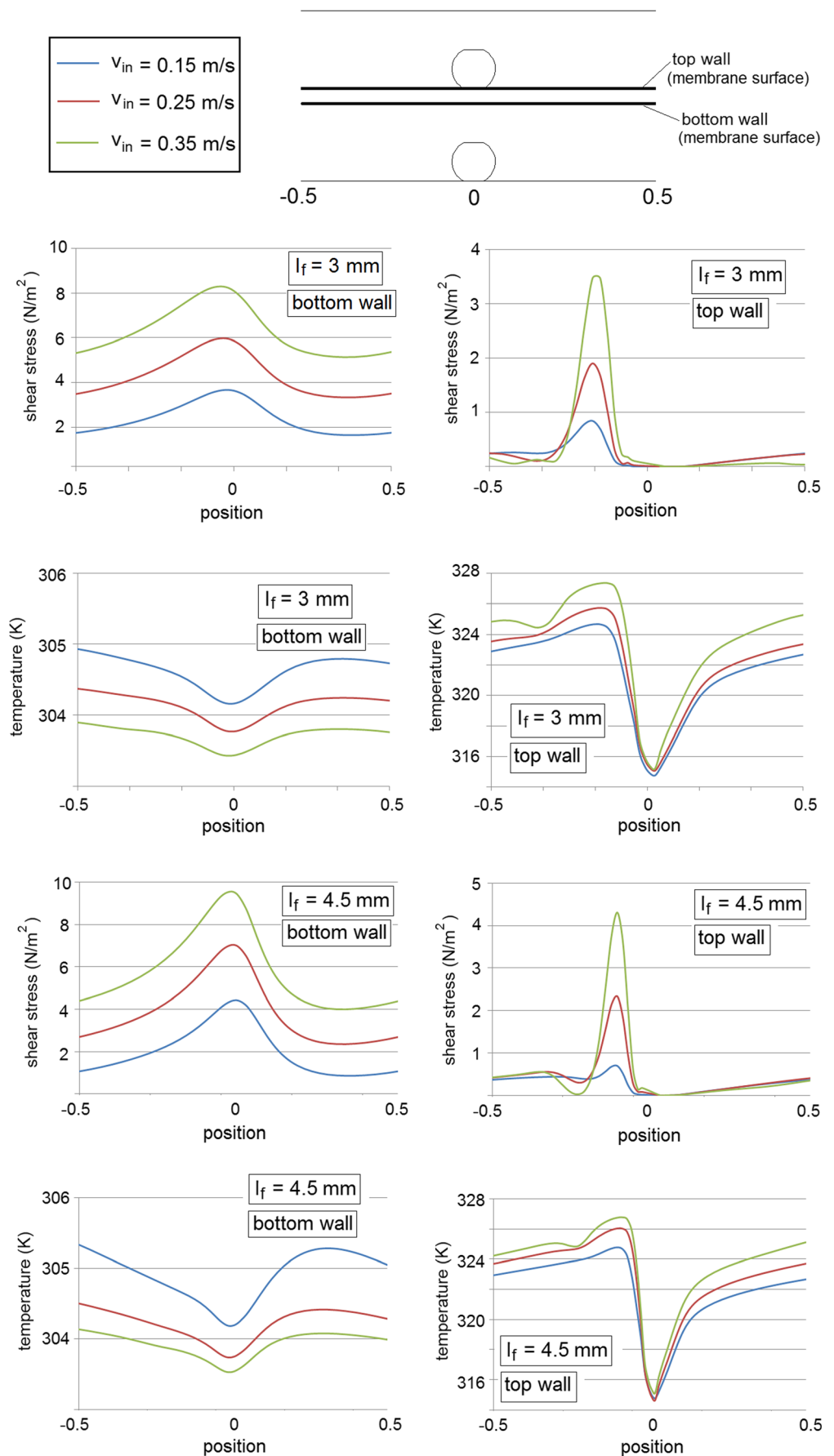


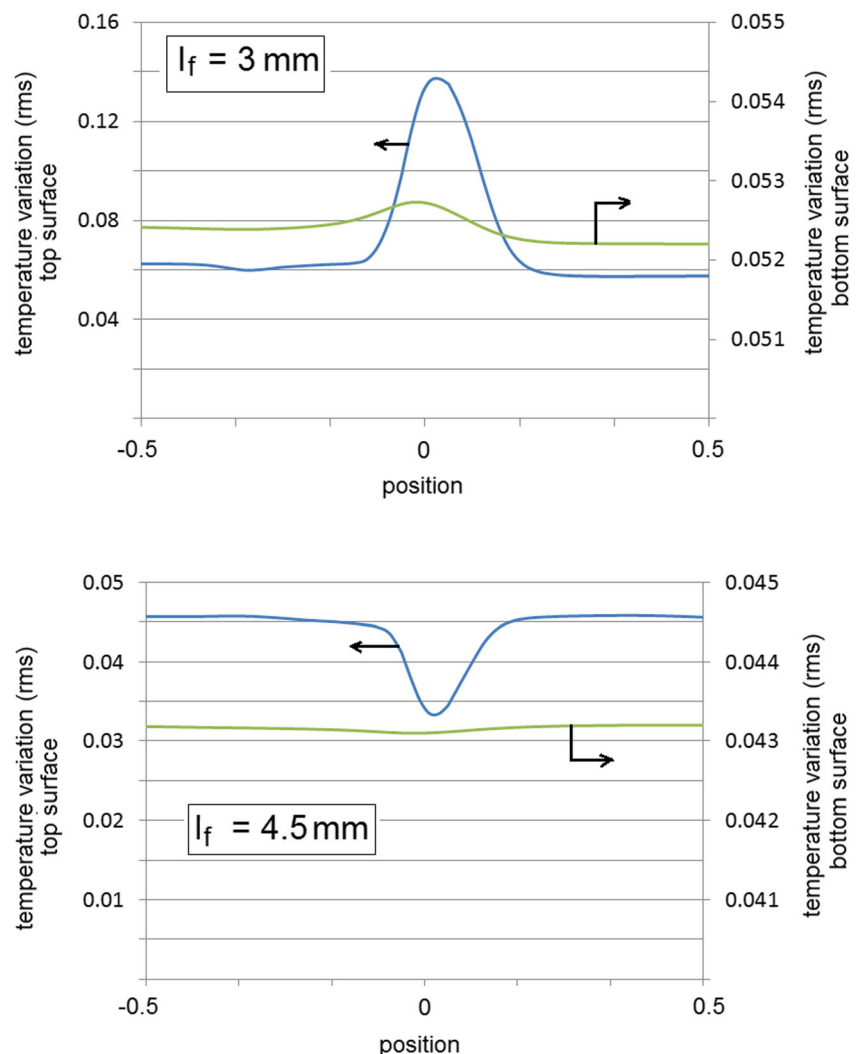
Fig. 5 Contours of velocity fluctuations / variations (RMS values) with time **a** $l_f = 3$ mm **b** $l_f = 4.5$ mm

Fig. 6 Distribution of shear stress and temperature on top and bottom membrane walls



vorticity magnitude increases in the major portion of the two channels. The increase in filament spacing also affects the vorticity within the feed and permeate channel. With the increase of spacing, the vorticity values relatively increase in the bottom portion as shown in Fig. 4. Higher velocity variations near the membrane can be useful in enhancing heat and mass transfer. The effect of filament spacing on unsteadiness in the membrane channels can be seen in Fig. 5. The unsteady behavior is absent in the beginning section of the channel for both the considered spacings. The approximate length for flow to be unstable is about two mesh lengths in the hot channel. In cold channel, the flow becomes transient after six filaments when spacing is 3 mm and after four filaments when spacing is 4.5 mm. The difference between the unsteady behavior in the top and bottom channels is due to the relatively low viscosity of the fluid in the hot channel. The variation of velocity with time is more when filament spacing is higher. The magnitude of velocity fluctuations (RMS values) is approximately up to 0.3 m/s when spacing/mesh length l_f is 4.5 mm whereas it is up to 0.2 m/s when l_f is 3 mm.

Fig. 7 RMS values of temperature fluctuations with time on top and bottom membrane surfaces



The shear stress and temperature profiles are shown in Fig. 6. The shear stress at the bottom membrane surface (in cold channel) increases as fluid flows with a high velocity above the filament. The location of maximum shear stress is slightly before the filament (at '0').

Approximately, at the same location, the local temperature decreases. The reduction in temperature on bottom membrane surface is desirable since it results in more heat transfer. The increase in inlet velocity increases the shear stress and decreases the temperature on the bottom surface but the shape/profile for the shear stress and temperature remains the same. It is, however, important to mention that the shear stress and the temperature plots are based on time-averaged results since the flow is unsteady at higher values of inlet velocities (0.25 and 0.35 m/s). On the top membrane surface, the shear stress is found higher at an approximate distance of $x/l_f = -0.15$ (measured from filament '0') where vorticity was seen higher in Fig. 3. The temperature at this maximum shear stress location is higher which is again desired. On the remaining portion of the top membrane surface, the shear stress is low due to low

velocity which significantly decreases the temperature. The pattern of shear stress and temperature variation with filament spacing of 4.5 mm is approximately the same. The variation in shear stress values is however relatively higher when spacing is 4.5 mm. For example, at a velocity of 0.15 m/s, the shear stress is between 1.7 and 3.8 N/m² when spacing is 3 mm whereas the range is 1.1–4.3 N/m² when spacing is 4.5 mm.

The temperature variation in time on the top and bottom membrane surface for the two considered spacings is shown in Fig. 7. The temperature plots show that the RMS of temperature fluctuation is more at the top membrane surface (i.e. on membrane surface in the hot fluid channel). On the bottom surface, the temperature variation is relatively less and remains almost constant. The local temperature varies more when the spacing is less i.e. 3 mm.

The effect of spacer configuration on heat transfer performance at two different velocities can be observed in Fig. 8. When spacer filaments are touching the bottom surface in both channels, the heat flux varies considerably. This behavior is seen for both the arrangements (inline and staggered) and both the spacings (3 and 4.5 mm). The heat flux reduces at

locations 0, 1 and 2 where the filaments in the hot channel are touching the membrane top surface. When filaments are on the opposite side of the membrane i.e. the filaments in the top channel are at the top and the filaments in the bottom channel are in the bottom portion, the heat flux values are more uniform and higher at different velocities and for both filament spacings which means less temperature polarization.

In Fig. 8, the time-averaged values of heat flux were shown. The changes in heat flux with time at a monitoring point in the middle of the channel are shown in Fig. 9. For all the cases it can clearly be noticed that flow is unstable as local heat flux has a periodic behavior. The period of repetition is 20–30 time steps for most of the cases. The staggered configuration with the spacing of 4.5 mm results in a relatively more or irregular heat flux variation.

The results shown in previous Figures were obtained through Direct Numerical Simulations (DNS) in which detailed flow features were predicted with respect to time. The DNS method though provides more accurate results but needs significant computational time. The time for simulation increases with the complexity of the case. An alternate method

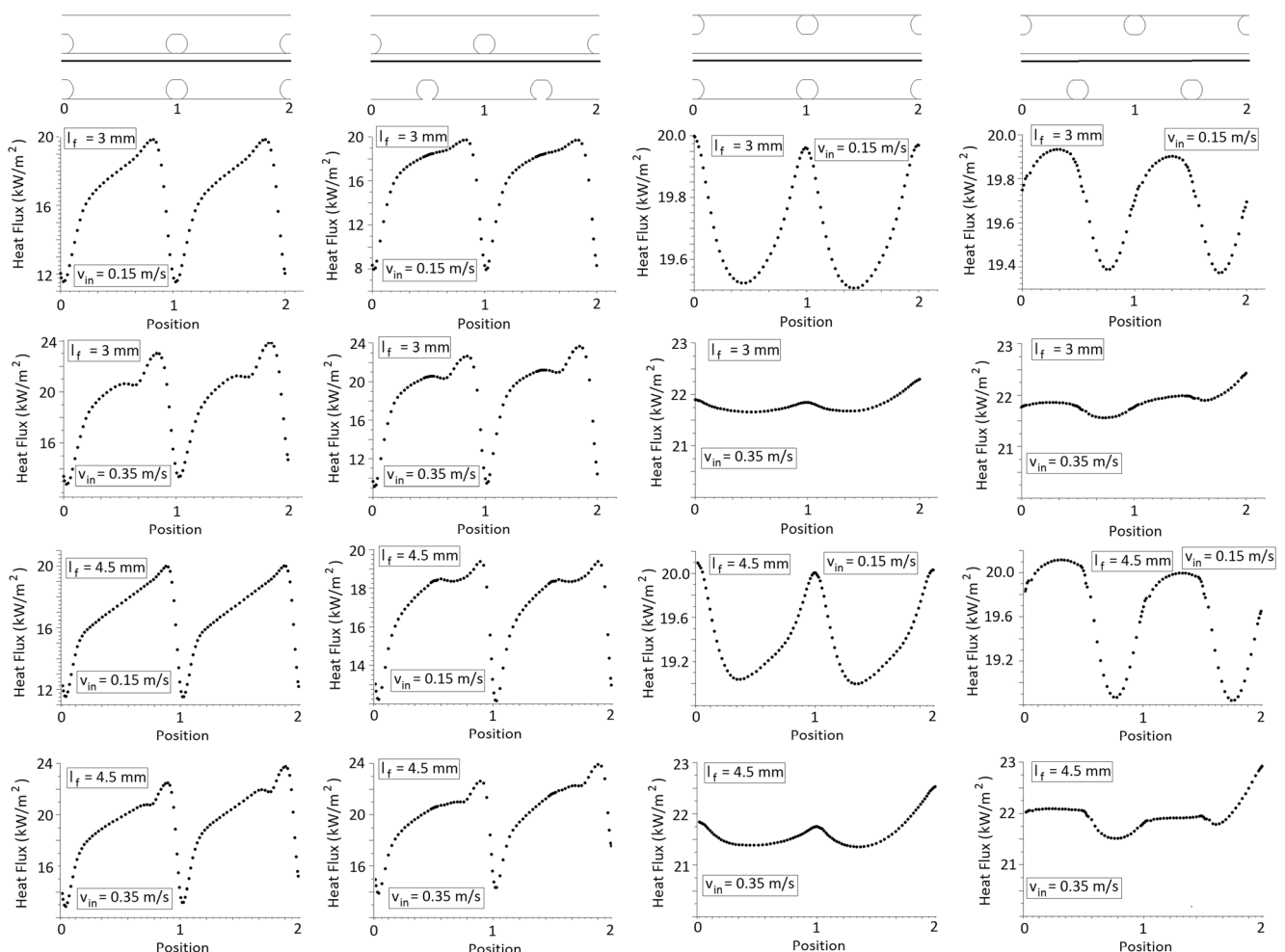


Fig. 8 Heat flux variation versus distance in different configurations

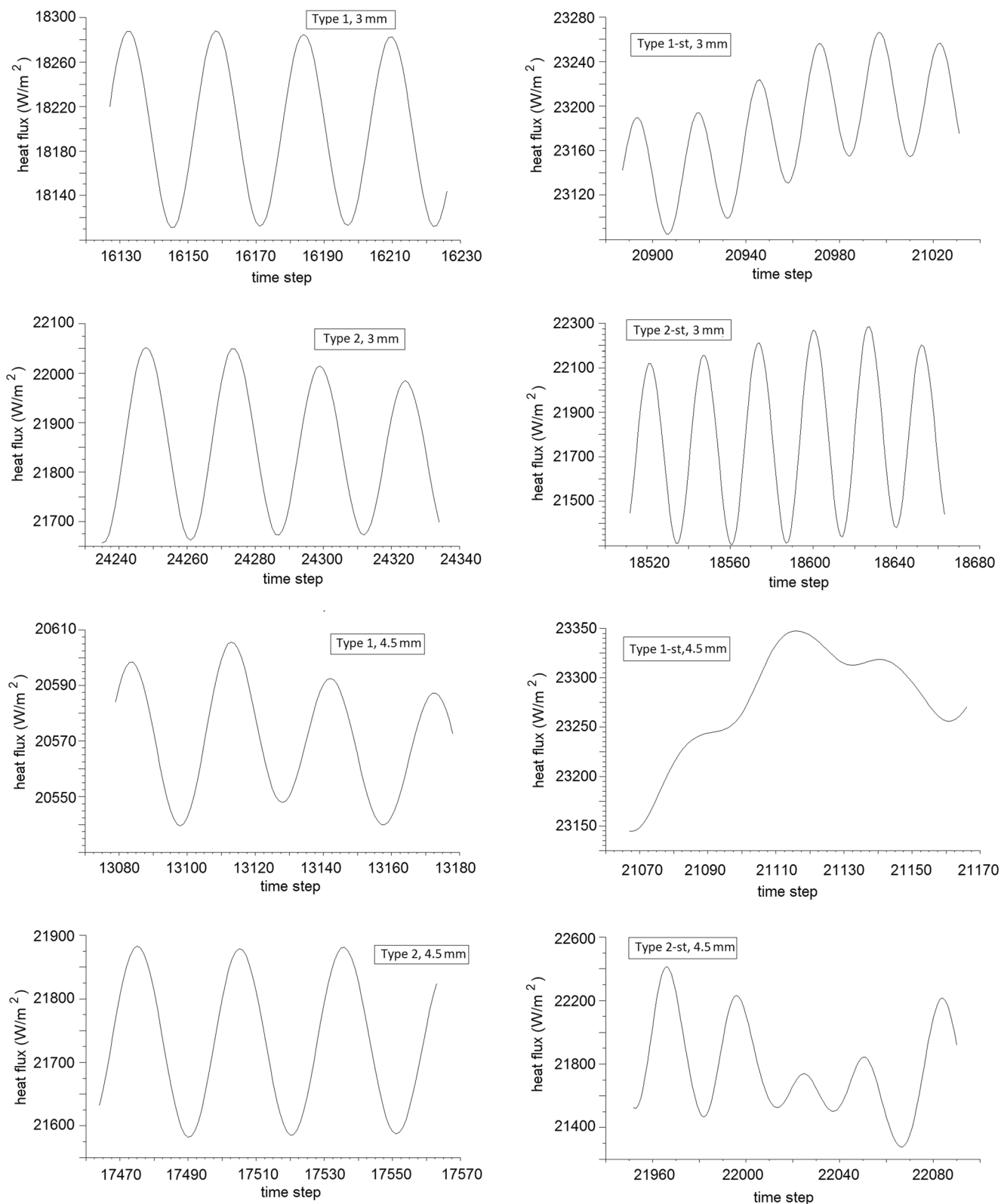


Fig. 9

Fig. 9 Local heat flux changes with respect to time in different configurations with inline and staggered arrangements

for examining transient/transitional flows in spacer-filled channel is to use a turbulence model as used in several studies

[25, 27, 28, 30]. The turbulence modeling approach provides time-averaged results for flow, heat transfer and turbulence

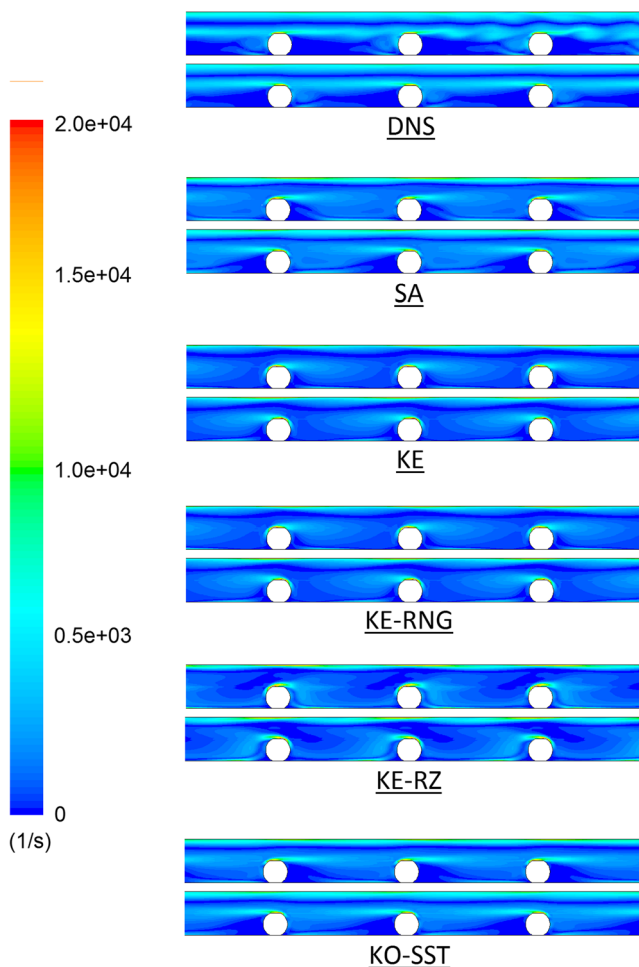


Fig. 10 Vorticity profiles using DNS approach and different turbulence models

parameters without simulating the flow oscillations in detail. There are several models for turbulent flows such as $k-\epsilon$ (KE), $k-\epsilon$ RNG (KE-RNG), $k-\epsilon$ Realizable (KE-RZ), $k-\omega$ (KO), $k-\omega$ Shear Stress Transport (KO-SST), Spalart-Allmaras (SA), etc. These models, however, should be evaluated and compared with experimental or DNS results before using for any particular problem. In the present research work, therefore, some models for fluid flow and heat transfer in membrane channels are proposed.

The comparison in terms of vorticity contours is shown in Fig. 10. The DNS method shows that the vorticity values are higher near the filaments and near the top surface of both channels and lower in the bottom portion of both the channels. The contours of vorticity obtained using various turbulence models do not perfectly compare with DNS results as vorticity is relatively higher in the bottom portion of channels. The SA and KO-SST models have however better similarity with DNS results than the other models.

The temperature profiles on the top and bottom membrane surfaces are shown in Fig. 11. Due to the stagnant zone at the filament (position '0') at the top membrane surface, the

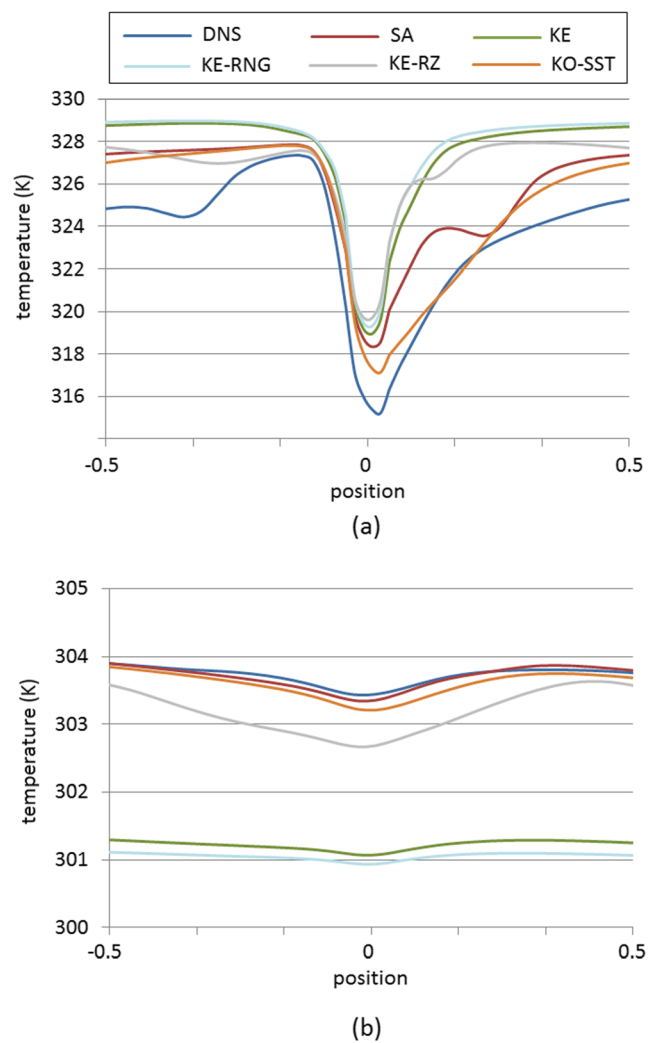


Fig. 11 Temperature plot on a top b bottom membrane surface obtained through simulations using DNS technique and turbulence models

temperature considerably drops as was seen in Fig. 6. The comparison of transient results with different turbulence models shows that the temperature plot of $k-\omega$ (SST) on the top surface is closest. The temperature profiles obtained

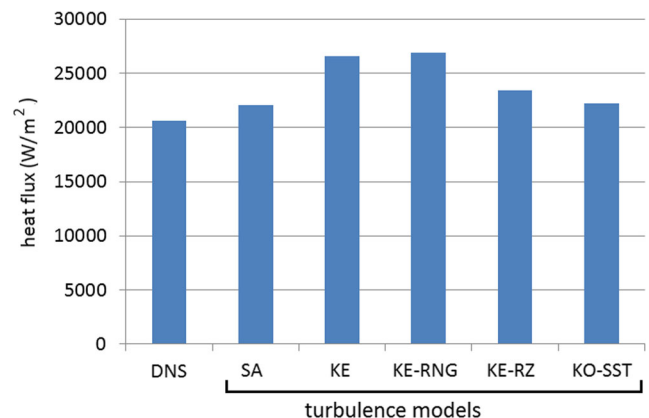
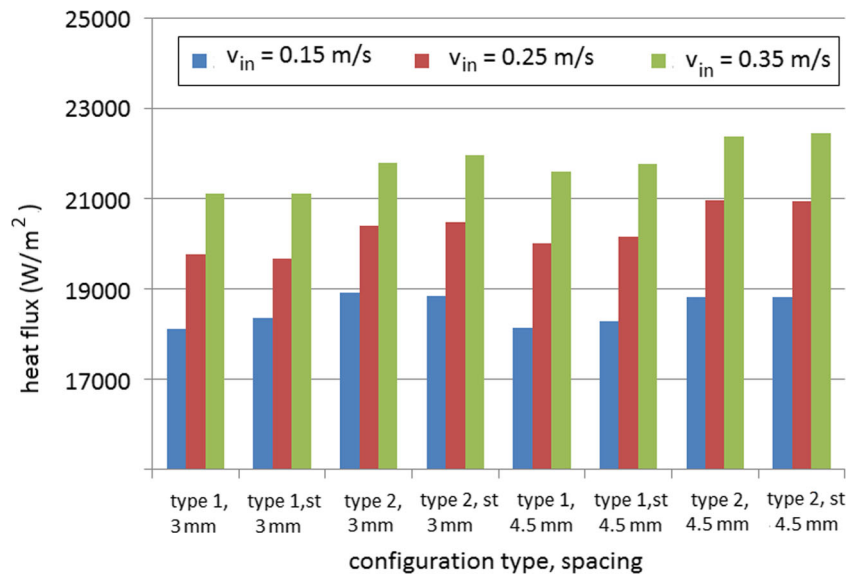


Fig. 12 Average heat transfer result found using DNS and turbulence modeling technique

Fig. 13 Average heat flux in different configurations versus inlet velocities



through various $k-\varepsilon$ models (KE, KE-RNG, KE-RZ) are significantly different. On the bottom membrane surface, the Spalart-Allmaras model predicts the temperature pattern better than $k-\omega$ (KO-SST) and the other models. The average heat flux in Fig. 12 shows that the Spalart-Allmaras model provides the most accurate results than the other models as the difference with DNS is least. The $k-\omega$ (SST) model and $k-\varepsilon$ (RZ) also yield reasonable results as the difference is less than 25%. The standard $k-\varepsilon$ and RNG variant may be considered less suitable for the considered range of Reynolds number as a significant difference is found in terms of heat transfer rates.

The comparison of various spacer arrangements at different velocities is shown in Fig. 13. The heat flux increases with inlet velocity or Reynolds number as expected. The increase is about 15% as velocity increases from 0.15 to 0.35 m/s. At higher velocity/Reynolds number however, the transient flow

can result in periodic disrupt of concentration and thermal boundary layer and removal of fouling agents. The comparison of spacer arrangement shows that type 2 is better than type 1 since the average heat fluxes are relatively higher. Secondly for both the types, the heat flux is higher when spacing is more i.e. 4.5 mm. The staggering of the filaments also enhances heat transfer in a few cases for example in type 1 ($l_f = 4.5$ mm). The configuration with transverse filaments opposite to the membrane layer with greater spacing can be considered more suitable for the membrane distillation process.

The present numerical results are also compared with the correlations proposed in previous experimental studies [13, 34]. From fluid properties and heat transfer rates/coefficients, Prandtl and Nusselt numbers are calculated respectively using Eqs. (3) and (4) and compared with experimental correlations (Eqs. (10) and (12)). The plot in Fig. 14 indicates that the

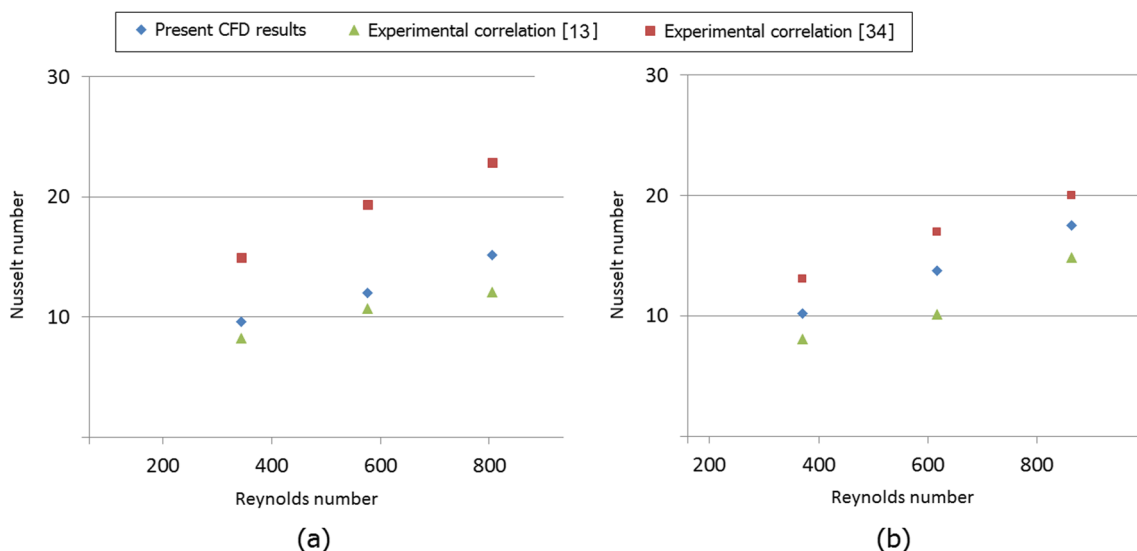


Fig. 14 Comparison of present CFD results with experimental results **a** $l_f = 3$ mm **b** $l_f = 4.5$ mm

Nusselt number values obtained using CFD are relatively higher when compared with ones obtained using Eq. (10). The comparison with Eq. (12) shows the CFD values are under-predicted. The difference is however between 20 and 40% for most of the cases. The present results can thus be considered satisfactory for determining the performance of various spacer types/arrangements.

4 Conclusions

The Computational Fluid Dynamics study in this paper shows that the spacer parameters like spacer configuration, arrangement (inline or staggered) and spacing affect the thermal and overall performance of the membrane distillation process. In the considered range of Reynolds number, the arrangement in which spacer filaments are touching the membrane surface is less useful since the variation in heat flux and temperature is more and average heat flux is less. The arrangement/orientation which has spacer filaments on the opposite side of the membrane results in higher heat transfer. The spacer with a greater spacing of 4.5 mm was also found to yield relatively higher heat transfer rates. The flow and heat transfer parameters are also determined through various turbulence models. The parameter values calculated using Spalart-Allmaras and $k-\omega$ (SST) turbulence models provide better agreement with DNS results. Finally, a fair agreement was found of present numerical results with experimental correlations in the literature.

Acknowledgements The support provided by NED University of Engineering and Technology, Karachi, Pakistan is acknowledged.

Compliance with ethical standards

Conflict of interest On behalf of all authors, the corresponding author states that there is no conflict of interest.

References

- González D, Amigo J, Suárez F (2017) Membrane distillation: perspectives for sustainable and improved desalination. *Renew Sustain Energy Rev* 80:238–259
- Martínez L, Vázquez-González MI, Florido-Díaz FJ (1998) Study of membrane distillation using channel spacers. *J Membr Sci* 144: 45–46
- Alkhudhiri A, Darwish N, Hilal N (2012) Membrane distillation: A comprehensive review. *Desalination* 287:2–18
- Drioli E, Ali A, Macedonio F (2015) Membrane distillation: recent developments and perspectives. *Desalination* 356:56–84
- Mahdi M, Shirazi A, Ismail AF, Matsuura T (2016) Computational fluid dynamic (CFD) opportunities applied to the membrane distillation process: state-of-the-art and perspectives. *Desalination* 377: 73–90
- Fimbres-Weihs GA, Wiley DE (2010) Review of 3D CFD modeling of flow and mass transfer in narrow spacer-filled channels in membrane modules. *Chem Eng Process* 49:759–781
- Katsandri A (2017) A theoretical analysis of a spacer filled flat plate membrane distillation modules using CFD: part II: temperature polarisation analysis. *Desalination* 408:166–180
- Chang H, Hsu J, Chang C, Ho C (2015) CFD study of heat transfer enhanced membrane distillation using spacer-filled channels. *Energy Procedia* 75:3213–3219
- Seo J, Kim YM, Kim JH (2017) Spacer optimization strategy for direct contact membrane distillation: shapes, configurations, diameters, and numbers of spacer filaments. *Desalination* 417:9–18
- Martínez L, Rodríguez-Maroto JM (2016) Characterization of membrane distillation modules and analysis of mass flux enhancement by channel spacers. *J Membr Sci* 274:123–137
- Martínez L, Vázquez-González MI, Florido-Díaz FJ (1998) Temperature polarization coefficients in membrane distillation. *Sep Sci Technol* 33:787–799
- Phattaranawik J, Jiratananon R, Fane AG, Halim C (2001) Mass flux enhancement using spacer filled channel in direct contact membrane distillation. *J Membr Sci* 187:193–201
- Phattaranawik J, Jiratananon R, Fane AG (2003) Effects of net-type spacers on heat and mass transfer in direct contact membrane distillation and comparison with ultrafiltration studies. *J Membr Sci* 217:193–206
- Chernyshov MN, Meindersma GW, de Haan AB (2005) Comparison of spacers for temperature polarization reduction in air gap membrane distillation. *Desalination* 183:363–374
- Cipollina A, Di Miceli A, Koschikowski J, Micale G, Rizzuti L (2011) CFD simulation of a membrane distillation module channel. *Desalin Water Treat* 6:177–183
- Cipollina A, Di Miceli A, Rizzuti L (2011) Membrane distillation heat transfer enhancement by CFD analysis of internal module geometry. *Desalin Water Treat* 25:195–209
- Al-Sharif S, Albeirutty M, Cipollina A, Micale G (2013) Modelling flow and heat transfer in spacer-filled membrane distillation channels using open source CFD code. *Desalination* 311:103–112
- Soukane S, Naceur MW, Francis L, Alsaadi A, Ghaffour N (2017) Effect of feed flow pattern on the distribution of permeate fluxes in desalination by direct contact membrane distillation. *Desalination* 418:43–59
- Yu H, Yang X, Wang R, Fane AG (2012) Analysis of heat and mass transfer by CFD for performance enhancement in direct contact membrane distillation. *J Membr Sci* 405–406:38–47
- Ahadi H, Karimi-Sabet J, Shariaty-Niassar M, Matsuura T (2018) Experimental and numerical evaluation of membrane distillation module for oxygen-18 separation. *Chem Eng Res Des* 132:492–504
- Guan G, Yao C, Lu S, Jiang Y, Yu H, Yang X (2018) Sustainable operation of membrane distillation for hypersaline applications: roles of brine salinity, membrane permeability and hydrodynamics. *Desalination* 445:123–137
- Eleiwi F, Ghaffour N, Alsaadi AS, Francis L, Laleg-Kirati TM (2016) Dynamic modeling and experimental validation for direct contact membrane distillation (DCMD) process. *Desalination* 384: 1–11
- Shakaib M, Hasani SMF, Ahmed I, Yunus RM (2012) A CFD study on the effect of spacer orientation on temperature polarization in membrane distillation modules. *Desalination* 284:332–340
- Jafarkhani M, Moraveji MK, Davarnejad R, Moztarzadeh F, Mozafari M (2012) Three-dimensional simulation of turbulent flow in a membrane tube filled with semi-circular baffles. *Desalination* 294:8–16
- Ranade VV, Kumar A (2005) Fluid dynamics of spacer filled rectangular and curvilinear channels. *J Membr Sci* 271:1–15

26. Ahmed S, Seraj MT, Jahedi J, Hashib MA (2011) CFD simulation of turbulence promoters in a tubular membrane channel. *Desalination* 276:191–198
27. Ahmad AL, Lau KK, Abu Bakar MZ (2005) Impact of different spacer filament geometries on concentration polarization control in narrow membrane channel. *J Membr Sci* 262:138–152
28. Cao Z, Wiley DE, Fane AG (2001) CFD simulations of net-type turbulence promoters in a narrow channel. *J Membr Sci* 185:157–176
29. Chen Z, Zhao B, Chen F, Li J (2013) Effect of the flow channel structure on the nanofiltration separation performance. *J Nanomater* 10:Article ID 132919, 10 pages
30. Li Y, Tung K, Lu M, Huang S (2009) Mitigating the curvature effect of the spacer-filled channel in a spiral-wound membrane module. *J Membr Sci* 329:106–118
31. Lawson KW, Lloyd DR (1997) Membrane distillation. *J Membr Sci* 124:1–25
32. Shakaib M, Ahmed I, Yunus RM (2011) Effect of permeation velocity on flow behavior and pressure drop in feed channels of membranes. In: ASEAN conference on scientific and social science research (ACSSSR2011)
33. White FM (2006) *Viscous fluid flow*, 3rd edn. McGraw-Hill, Boston
34. Schock G, Miquel A (1987) Mass transfer and pressure loss in spiral wound modules. *Desalination* 64:339–352

Publisher's note Springer Nature remains neutral with regard to jurisdictional claims in published maps and institutional affiliations.